

# DUST CONTENT, GALAXY ORIENTATIONS, AND SHAPE NOISE IN IMAGING SURVEYS

PETCHARA PATTARAKIJWANICH

Department of Astrophysical Sciences, Princeton University, Princeton, NJ 08544, USA

FABIAN SCHMIDT

Max-Planck-Institute for Astrophysics, D-85748 Garching, Germany

*Draft version March 3, 2022*

## ABSTRACT

We show that dust absorption in disk galaxies leads to a color- and orientation-dependent centroid shift which is expected to be observable in multi-band imaging surveys. This centroid shift is an interesting new probe which contains astrophysically and cosmologically relevant information: it can be used to probe the dust content of a large sample of galaxies, and to reduce the shape noise due to inclination of disk galaxies for weak lensing shear. Specifically, we find that data sets comparable to CFHTLenS, the Dark Energy Survey (DES) or the Hyper Suprime-Cam (HSC) survey should provide a dust measurement for several hundred galaxies per square degree. Conversely, given knowledge of the dust optical depth, this technique will significantly lower the shape noise for the brightest galaxies in the sample (signal-to-noise greater than a few hundred), thereby increasing their relative importance for the weak lensing shear measurement.

## 1. INTRODUCTION

Observational cosmology is currently benefiting from an enormous growth in large photometric survey data sets, as delivered by the CFHTLenS<sup>1</sup>, Hyper Suprime-Cam (HSC)<sup>2</sup> survey, Dark Energy Survey (DES)<sup>3</sup>, KiDS<sup>4</sup> and other surveys. These state of the art surveys deliver images in several bands for a hundred million galaxies or more. Currently, these data sets are exploited primarily through three observables: image shapes, which are used to measure weak gravitational lensing shear; galaxy number counts, used to measure angular auto- and cross-correlation functions; and image magnitudes in different bands, which are the input for photometric redshift estimation.

In this paper, we show that the image centroid measured in different bands can also serve as a valuable source of cosmological information. In particular, it can be used to infer the dust content of galaxies, and to infer the orientation of disk galaxies independently of their observed shape. The underlying idea is that dust absorption modifies galaxy images by a different amount in different bands. The most easily observable of these modifications is a *shift in the centroid* of the image between different bands. As we will show, a radial gradient in the disk plane of the optical depth is sufficient to produce such a centroid shift, which is approximately proportional to the tangent of the inclination angle.

Direct measurements of the optical depth due to dust absorption through the disk of spiral galaxies has mainly been done using two techniques. The first is to observe occulting galaxy pairs, where comparing the unobscured part to the obscured part of the background galaxy can give information on the transparency of the foreground

one (e.g., White et al. 2000). The second approach is through the number count of distant background galaxies observed through the disk of local face-on galaxies (e.g., Holwerda et al. 2013). Both of these methods rely on spatially resolved observation, limiting the number of galaxies studied this way to only tens in the local universe.

There are other ways to indirectly infer the dust optical depth in galaxies. Far-IR spectral energy distributions from Spitzer and Herschel can be used to measure total dust emission, implying the total dust mass and expected obscuration in the optical. However, relating the FIR SED to optical depth in visible wavelength is not straightforward due to the uncertainty in dust models (e.g., Draine et al. 2007). Dust content in late-type galaxies can be determined by detailed modeling of photometric and spectroscopic data in small samples of nearby galaxies (see Calzetti 2001 for a review). A similar approach that works in a statistical sense (i.e. averaged over many galaxies) with spatially-unresolved data is to fit stellar populations using optical spectra, and then infer dust reddening from the discrepancy between the observed photometry and the best-fit model (e.g., Kauffmann et al. 2003). Even though this can be done for a large number of galaxies from surveys, the uncertainty is large due to the systematics in stellar population modeling.

Effects of inclination-dependent obscuration have been considered by a number of authors. Shao et al. (2007) showed that the luminosity function of spiral galaxies depends on inclination in the expected way, then determined the inclination-corrected luminosity function. Chevillard et al. (2013) determined the dust content of nearby star-forming galaxies using fits to the optical/NIR photometry with sophisticated radiative transfer model taking this effect into account. Yip et al. (2011) considered the possible biases induced by inclination-dependent reddening on derived photometric redshift.

<sup>1</sup> <http://www.cfhtlens.org/>

<sup>2</sup> <http://www.subarutelescope.org/Projects/HSC/>

<sup>3</sup> <http://www.darkenergysurvey.org/>

<sup>4</sup> <http://kids.strw.leidenuniv.nl/>

The centroid shift we describe in this paper is an important new observable which is able to break degeneracies present when simultaneously estimating the dust content and galaxy orientation. Thus, by using this technique in conjunction with the previously developed ones, one can expect to obtain estimates for the dust that are significantly more robust.

The degeneracy between an elliptical appearance due to inclination of a disk galaxy and the ellipticity induced by weak lensing along the line of sight is the main source of noise in shear measurements. Thus, any independent constraint on the orientation of a disk galaxy can increase the signal-to-noise of shear measurements. This is especially relevant since disk galaxies typically make up the majority of galaxies in flux-selected samples from imaging surveys. We show how (noisy) information on the orientation, in our case from the centroid shift, can be included in the shear estimate from galaxy shapes. This could also be useful in other contexts, for example when incorporating orientation information from spectra (Huff et al. 2013).

The outline of the paper is as follows. In Sec. 2, we present the calculation of the centroid shift due to dust absorption in disk galaxies. We perform both a numerical solution of the radiative transfer problem as well as an analytical estimate. Sec. 3 then shows how the information on the galaxy orientation can be incorporated in shear estimation to lower the shape noise. We then briefly describe the constraints on the dust content that can be obtained via this technique. We conclude in Sec. 5. The appendices present further details on analytical estimates and the expected accuracy of centroid measurements in imaging surveys.

## 2. CENTROID SHIFT FROM DUST EXTINCTION

In this section, we use a simplified radiative transfer calculation to show why dust extinction in disk galaxies leads to a relative centroid shift between different bands. For this, we will ignore scattering. The radiative transfer equation then simplifies to

$$\frac{dI_\nu(\mathbf{x}(s), \hat{\mathbf{n}})}{ds} = -\kappa_\lambda(\mathbf{x}(s))I_\nu(\mathbf{x}(s), \hat{\mathbf{n}}) + \epsilon_\lambda(\mathbf{x}(s), \hat{\mathbf{n}}), \quad (1)$$

where  $I_\nu$  is the photon intensity,  $\hat{\mathbf{n}}$  is the unit photon momentum vector,  $s$  is the line element,  $\mathbf{x}(s)$  is the position along the ray, and  $\kappa_\lambda$ ,  $\epsilon_\lambda$  are the opacity and emissivity, respectively. In the following, we will drop the subscript  $\lambda$  for clarity. We will assume an isotropic opacity  $\kappa$  and emissivity  $\epsilon$ , and correspondingly drop the argument  $\hat{\mathbf{n}}$  throughout. The solution to Eq. (1) is then given by

$$I(s) = \int_{-\infty}^s ds' \epsilon(\mathbf{x}(s')) \exp \left[ - \int_{s'}^s \kappa(\mathbf{x}(s'')) ds'' \right]. \quad (2)$$

Let us consider a galaxy with cylindrical symmetry, so that in cylindrical coordinates around the galaxy center [“galaxy frame”,  $(r_{\text{gf}}, z_{\text{gf}}, \varphi)$ ] we can write  $\epsilon(\mathbf{x}) = \epsilon(r_{\text{gf}}, z_{\text{gf}})$  and  $\kappa(\mathbf{x}) = \kappa(r_{\text{gf}}, z_{\text{gf}})$ . Consider a ray that intersects the  $z_{\text{gf}} = 0$  plane (“the disk”, see Fig. 1) at  $(x_{\text{gf}}, y_{\text{gf}})$ , which we define as  $s = 0$ , at an angle  $\theta$  with the  $z_{\text{gf}}$  axis. The angle  $\theta$  corresponds to the inclination angle as seen by a distant observer, with  $\theta = 0$  corresponding to a face-on view and  $\theta = \pi/2$  being edge-on.

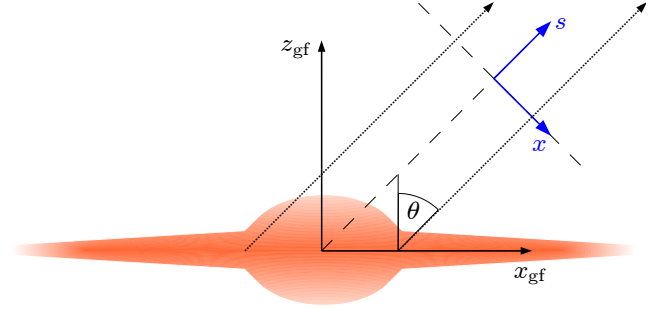


**Figure 1.** Geometry of the galaxy and lines of sight. The black coordinate system shows the galaxy frame (“gf”) while the blue coordinate axes denote the observer system  $(x, y)$  on the sky plane (the  $y$  axes of both coordinate systems are perpendicular to the figure).  $\theta$  is the inclination angle, and we have set  $\varphi = 0$ . The two lines of sight (dotted) at  $\pm|x|$  in the observer frame pass through different amounts of material and thus experience difference extinction.

This yields

$$z_{\text{gf}}(s) = s \cos \theta; \quad r_{\text{gf}}(s) = ((x_{\text{gf}} + s \sin \theta)^2 + y_{\text{gf}}^2)^{1/2}. \quad (3)$$

We can replace  $s$  with  $z$  (provided that  $\theta \neq \pi/2$ ). Further, we are interested in the flux  $f_{\text{obs}} \propto I_{\text{obs}}$  far away from the galaxy, and thus let  $s \rightarrow \infty$ . Eq. (2) becomes

$$I_{\text{obs}}(\theta, x_{\text{gf}}, y_{\text{gf}}) = \frac{1}{\cos \theta} \int_{-\infty}^{\infty} dz_{\text{gf}} \epsilon(r_{\text{gf}}(z_{\text{gf}}), z_{\text{gf}}) \quad (4)$$

$$\times \exp \left[ - \frac{1}{\cos \theta} \int_z^{\infty} \kappa(r_{\text{gf}}(z'), z') dz' \right],$$

where

$$r_{\text{gf}}(z_{\text{gf}}) = [(x_{\text{gf}} + z_{\text{gf}} \tan \theta)^2 + y_{\text{gf}}^2]^{1/2}. \quad (5)$$

Evaluating this expression yields the appearance of the disk with inclination angle  $\theta$  as seen by a distant observer. For this purpose, we define a coordinate system on the sky  $(x, y)$ , assuming the flat-sky approximation, centered on the true center of the galaxy and scaled with the angular diameter distance to the galaxy. The mapping between  $(x, y)$  and  $(x_{\text{gf}}, y_{\text{gf}})$  then is

$$\begin{pmatrix} x_{\text{gf}} \\ y_{\text{gf}} \end{pmatrix} = \begin{pmatrix} x \cos \theta \cos \varphi_i - y \cos \theta \sin \varphi_i \\ y \cos \varphi_i + x \sin \varphi_i \end{pmatrix}. \quad (6)$$

where  $\varphi_i$  is the azimuthal angle of the inclination axis.

### 2.1. Numerical Evaluation

In the following, we perform a numerical integration of the radiative transfer solution Eq. (4) for the case when both the absorbing and emitting components of the galaxy follow a double exponential distribution in  $r_{\text{gf}}$  and  $z_{\text{gf}}$ ,

$$\epsilon(r_{\text{gf}}, z_{\text{gf}}) = \epsilon_0 e^{-r_{\text{gf}}/r_\epsilon} e^{-|z_{\text{gf}}|/z_\epsilon}$$

$$\kappa(r_{\text{gf}}, z_{\text{gf}}) = \kappa_0 e^{-r_{\text{gf}}/r_\kappa} e^{-|z_{\text{gf}}|/z_\kappa}. \quad (7)$$

Assuming this model, Eq. (4) can be evaluated numerically for any set of parameters. The emissivity normalization  $\epsilon_0$  and the absolute scale length  $r_\epsilon$  do not need to be specified, since they only scale the solution in a trivial way. The relevant quantities are the opacity  $\kappa_0$  and the

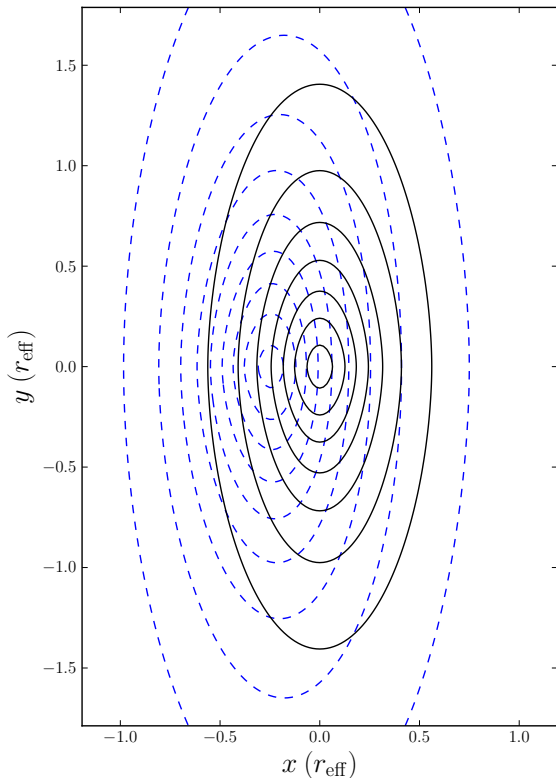


**Figure 2.** Contours showing the appearance of the disk with (blue dashed) and without (black solid) the effect of dust obscuration. Inclination angle here is  $\theta = 70^\circ$ . The disk parameters used here are the fiducial set of parameters [Eq. (8)] except for the optical depth which is boosted from  $\tau_{\text{fo}} = 0.5$  to 5.0 to show the effect clearly. The axes are scaled to the effective radius  $r_{\text{eff}}$  (half-light radius) for a face-on view.

ratios of the scale lengths and heights. We estimate the value of  $\kappa_0$  from the face-on optical depth,  $\tau_{\text{fo}}$ , which is the optical depth corrected for inclination and averaged over the inner  $2r_\epsilon$  (approximately one effective radius, consistent with how it is measured in the literature, see Calzetti (2001) for a review). In the following, we assume the values of optical depths in B- and I-bands and ratios of scales to be

$$\begin{aligned} \tau_{\text{fo,B}} &\simeq 0.5 \\ \tau_{\text{fo,I}} &\simeq 0.2 \\ z_\epsilon/r_\epsilon &\simeq 0.2 \\ r_\kappa/r_\epsilon &\simeq 1.4 \\ z_\kappa/z_\epsilon &\simeq 0.5. \end{aligned} \quad (8)$$

These values of optical depths are typical for Sb-Scd galaxies summarized by Calzetti (2001) (see however Driver et al. (2007) who obtain somewhat larger values). Note that these values are for optically-selected low-redshift galaxies and there is evidence that infrared-selected galaxies and galaxies at higher-redshift have significantly larger optical depths (Grootes et al. 2013; Boquien et al. 2013; Sargent et al. 2010). Therefore it is well possible that the galaxies detected in deep imag-

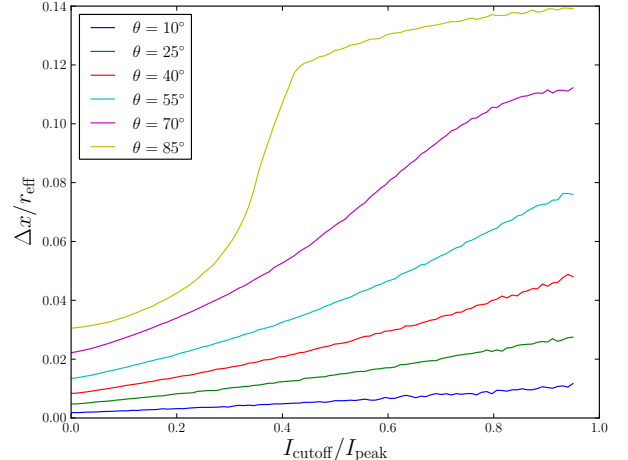


**Figure 3.** The magnitude of the fractional centroid shift  $\Delta x/r_{\text{eff}}$  as a function of cutoff surface brightness (in units of the peak value at the galaxy center) of the region used to measure the centroid. The different lines show the same disk from different inclination angles. The disk parameters are given in Eq. (8) with  $\tau_{\text{fo}} = 0.5$ .

ing surveys will show larger values of  $\tau_{\text{fo}}$ . The values used for ratios of scale lengths and heights are representative of what is found in the literature, where they are derived from analysis of edge-on local spiral galaxies (Byun et al. 1994; Xilouris et al. 1999; Bianchi 2007; Gadotti et al. 2010). Despite the significant variation from galaxy to galaxy, all measurements consistently suggest that  $z_\kappa/z_\epsilon < 1$ , i.e., the source of attenuation is more concentrated to the disk than the emission. We show in Sec. 2.2 that this ratio governs the sign of centroid shift, and therefore our fiducial model with fixed parameters is still qualitatively robust despite possible variations in these parameters.

With the surface brightness at each position  $(x, y)$  on the sky-plane projection of the disk calculated, one can explore how the extinction affects the appearance of the disk in different bands. The appearance of the disk in one band is shown in Fig. 2. The solid black contour shows the disk if no dust is present, while the blue dashed contour includes the effect of dust extinction. The disk shown in this figure is at inclination angle  $\theta = 70^\circ$  with our fiducial set of parameters except for the dust optical depth, which is boosted by a factor of 10 to  $\tau_{\text{fo}} = 5.0$  in order to show the effect more clearly.

The effect of extinction shifts the radiation systematically to one side, as expected because the radiation from one side goes through thicker column of absorber than the other. As dictated by symmetry, the shift is perpendicular to the axis around which the galaxy is rotated. The amount of shifting, however, is not uniform across the disk but depends on each surface brightness level. The bright, central part is shifted by a larger fractional amount than the fainter part. This is a consequence of the larger extinction gradient toward the center of the galaxy. To explore this effect, we divide the simulated disk image into isophotes (contours of constant surface brightness), and plot the shift of isophotes above some surface brightness threshold as a function of threshold value (see Fig. 3). Here and throughout, we scale the centroid shift to the effective radius  $r_{\text{eff}}$ , or half-light ra-

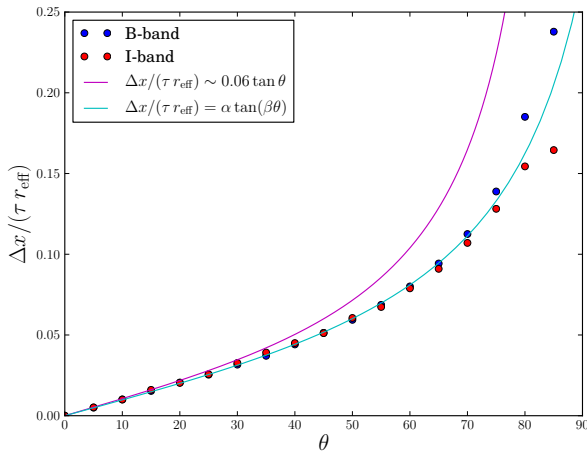


**Figure 4.** Fractional centroid shift calculated for both the *B*-band ( $\tau_{\text{fo}} = 0.5$ , blue point) and the *I*-band ( $\tau_{\text{fo}} = 0.2$ , red point). The shifts are normalized by the optical depth in each respective band to show the linear dependence. The magenta line is the analytic approximation discussed in Sec. 2.2, which agrees with the full numerical evaluation at small inclinations as expected. The cyan line is the functional fit to both sets of points [Eq. (10)], which we used as the fiducial relation between the shift and inclination angle.

dus, the radius within which one half of the total luminosity of the galaxy is emitted. This radius is related to the radial scale length  $r_\epsilon$  approximately by  $r_{\text{eff}} \sim 1.7r_\epsilon$ . As the threshold increases, we only calculate the centroid from the brightest part of the disk, and the centroid shift grows as expected. For the almost edge-on disk, a strongly non-linear behavior is apparent.

In Fig. 4, we show the centroid shift, measured within  $0.5r_{\text{eff}}$  (for reasons fully explained in Sec. 2.3) scaled to the effective radius  $r_{\text{eff}}$  and the optical depth  $\tau_{\text{fo}}$ , as a function of inclination angle. We see that the centroid shift can be well approximated as linear in  $\tau_{\text{fo}}$ . The two lines show the analytical approximation presented in the next section, and a parametrization which we will use for the following results.

## 2.2. Analytical estimates

The physical reason for the centroid shift can be inferred from Fig. 1, where we have let the  $y$  axis (perpendicular to the page) be the orientation axis of the galaxy. A ray emitted towards the observer from the negative  $x$  axis passes through matter closer to the center than the opposite ray from the positive  $x$  axis. This means that it will experience more emission and absorption than the latter; which contribution dominates depends on the configuration of absorbing and emitting material. Since the  $x > 0$  half of the galaxy image now has a different flux than the  $x < 0$  half, the centroid of the observed image, i.e. the center-of-mass of the light distribution, is shifted from the  $x = 0$  position of the actual galaxy center. Of course, for  $\theta = 0$  both rays pass through equivalent emission and absorption (on average), and there will be no centroid shift. More generally, both a radial and  $z$ -gradient is necessary in *either* the opacity or emissivity.

An analytical calculation of the centroid shift can be performed for small inclination angle, by expanding Eq. (4) to linear order in  $\tan \theta$ . The details of this are

given in Appendix A. For the fiducial parameters Eq. (8), the centroid shift is along the negative  $x$ -axis, i.e. the effect of more emission at smaller radii wins over the higher absorption. This is due to the more concentrated distribution of opacity as compared to the emissivity; while the former is dominated by gas clouds largely confined to the disk, the latter also receives contributions from older stellar populations which are more extended. Quantitatively, the analytical estimate yields [Eq. (A19)]

$$\frac{\Delta x_{\text{cen}}}{r_{\text{eff}}} \simeq -0.06 \tan \theta \tau_{\text{fo}}. \quad (9)$$

This linear approximation is compared to the direct numerically evaluated result in Fig. 4. For inclination angles less than about 45 degrees, the numerical results follow  $\tan \theta$  closely. Moreover, the coefficient of the analytical estimate, which uses some simplifications in various weighting integrals, agrees with the numerical result to better than 10%.

## 2.3. Parametrization of centroid shift

For the purpose of forecasting how well the centroid shift can be measured in imaging surveys, we need a parametrization of the centroid shift as a function of optical depth  $\tau_{\text{fo}}$  and inclination  $\theta$ . Since the effect depends on isophote level (Fig. 3), the first step is to devise an optimal centroid estimator for the purpose of measuring the centroid shift, which is described by a radial weight function  $w(r)$ . This derivation is given in Appendix B. It turns out that this kernel is strongly peaked at small radii, so that, for all but the most highly resolved galaxies, most of the information on the centroid shift is contained in the innermost resolved region around the centroid of the galaxy, i.e. within one full-width-half-maximum radius  $r_{\text{PSF}}$  of the point-spread function (PSF).

We then measure the centroid shift within  $r_{\text{PSF}}$  in the simulated galaxy image as a function of inclination. In a realistic galaxy survey, one has to take into account that differently resolved galaxies will have different centroid shifts. For the sake of simplicity, and to conservatively estimate the effect for galaxy samples used for weak lensing, we will consider a poorly-resolved galaxy with  $r_{\text{eff}} = 2r_{\text{PSF}}$  in the following. This is a conservative assumption since a better-resolved galaxy will yield a larger centroid shift.

In order to provide an accurate description even for very inclined galaxies, we use a fit function to describe the dependence on  $\theta$ . We found that the magnitude of the fractional centroid shift is well fitted by a function of the form

$$\frac{|\Delta x_{\text{cen}}|}{r_{\text{eff}}} = F(\tau_{\text{fo}}, \theta) \\ F(\tau_{\text{fo}}, \theta) = \alpha \tau_{\text{fo}} \tan(\beta \theta), \quad (10)$$

where  $\alpha = 0.066$  and  $\beta = 0.85$ , which is a slight generalization of the analytical result given in the previous section. The fit function is compared with the numerical result in Fig. 4 and is found to represent the centroid shifts well in both bands.

## 2.4. Measuring orientation

With the relationship between inclination angle and the centroid shift calibrated, it is now possible to use this information to measure the orientation of a disk from images in two bands (called band  $a$  and  $b$  respectively, which in this case our fiducial model parameters are from  $B$ -band and  $I$ -band). This orientation measurement assumes that the optical depth is known for the given galaxy; the converse case, i.e., inferring the optical depth from the centroid shift when assuming a certain orientation, is considered in Sec. 4. Further, we also assume that there is no scatter in the optical depths and scale ratios [Eq. (8)] that control the centroid shift at fixed inclination. In reality, there can be significant variation in these parameters and the empirical relation calculated in section 2.3 can be thought of as a median relationship.

Consider a disk galaxy with an inclination angle  $\theta$ , and azimuthal angle  $\phi$  with respect to a fixed direction  $\mathbf{i}$  on the sky. We will denote positions on the sky (approximated as flat) with  $\mathbf{x}$  here. The centroid position in each band will be shifted from the unknown true position by

$$\begin{aligned}\mathbf{x}_a &= x_a \mathbf{i} + y_a \mathbf{j} = F(\tau_a, \theta) (-\cos \phi \mathbf{i} + \sin \phi \mathbf{j}) r_{\text{eff},a} \\ \mathbf{x}_b &= x_b \mathbf{i} + y_b \mathbf{j} = F(\tau_b, \theta) (-\cos \phi \mathbf{i} + \sin \phi \mathbf{j}) r_{\text{eff},b},\end{aligned}$$

where  $F(\tau_{\text{fo}}, \theta)$  is defined in Eq. (10), and  $\tau_{a,b}$  denote the optical depths  $\tau_{\text{fo}}$  of the galaxy in each band.

What we measure is the differential shift between the two bands given by

$$\Delta \mathbf{x} = \Delta x \mathbf{i} + \Delta y \mathbf{j} = F(\tau_a - \tau_b, \theta) (-\cos \phi \mathbf{i} + \sin \phi \mathbf{j}) r_{\text{eff}}. \quad (11)$$

where we have used that the shift is linear in  $\tau$ , and assumed that the effective radii of the galaxy in each band are approximately equal; the latter assumption is merely for the sake of simplicity and can be easily dropped.

By assuming a value for  $\tau_a - \tau_b$ , the angles  $\theta$  and  $\phi$  can then be solved for through

$$\begin{aligned}\theta &= [F^{-1}] \left( \tau_a - \tau_b, \frac{\sqrt{\Delta x^2 + \Delta y^2}}{r_{\text{eff}}} \right) \\ &= \frac{1}{\beta} \arctan \left( \frac{\sqrt{\Delta x^2 + \Delta y^2}}{\alpha(\tau_a - \tau_b) r_{\text{eff}}} \right) \\ \phi &= \arctan \left( -\frac{\Delta y}{\Delta x} \right),\end{aligned} \quad (12)$$

where  $[F^{-1}]$  denotes the inverse function (with respect to  $\theta$ ) of Eq. (10), given explicitly in the second line.

In order to obtain quantitative forecasts for the information contained in the centroid shifts, we also need an estimate of the observational uncertainty of the centroid shift measured in actual imaging surveys. For this, we performed a study using simulated HST imaging (Massey et al. 2007) which is described in detail in App. C. The fractional uncertainty in centroid position is approximately given by

$$\text{RMS} \left( \frac{x, y}{r_{\text{eff}}} \right) = \frac{3.3}{\nu}, \quad (13)$$

where  $\nu$  is the signal-to-noise of the galaxy image. In other words, the uncertainty in each of the centroid components for a galaxy measured at  $\nu = 10$  is roughly one

quarter of the effective radius. We will use this estimate for the numerical studies presented in the next section.

### 3. IMPROVING SHEAR ESTIMATION

We now derive how the orientation information contained in the centroid shift can be used to reduce shape noise in weak lensing shear estimation of disk galaxies. This corresponds to an increase in the information of weak lensing shear surveys at no observational cost, and could thus be highly relevant to ongoing and upcoming imaging surveys.

Our goal is to construct the posterior

$$P(\boldsymbol{\gamma} | \hat{\Delta \mathbf{x}}, \hat{I}_{\text{sky}}), \quad (14)$$

where  $\boldsymbol{\gamma} = (\gamma_1, \gamma_2)$  is the shear vector and  $\hat{\Delta \mathbf{x}}, \hat{I}_{\text{sky}}$  denote the measurements of the centroid shift and second moment tensor of the galaxy image, respectively. For the sake of simplicity, we will assume no noise in the measurement of  $\hat{I}_{\text{sky}}$ , since this is not the main focus of the paper and can be straightforwardly included in the approach described here. In full generality, we have to allow for magnification as well. We assume however that we have no knowledge about the intrinsic size of the galaxy, so that marginalizing over the intrinsic size will remove all information on the magnification. To simplify the derivation, we will thus ignore the magnification and only work with the two components of the shear. Specifically, we use the shear parametrization of Bernstein and Jarvis (2002), in which the symmetric unit-determinant shear matrix is given by

$$S_{\boldsymbol{\eta}} = R_{\varphi} \begin{pmatrix} e^{\eta/2} & 0 \\ 0 & e^{-\eta/2} \end{pmatrix} R_{\varphi}^T, \quad (15)$$

where  $\boldsymbol{\eta}$  is the conformal shear vector,  $\eta = |\boldsymbol{\eta}|$ , and  $\varphi$  is the azimuthal angle of  $\boldsymbol{\eta}$ .  $R_{\varphi}$  denotes a rotation by  $\varphi$  around the line of sight. Note that in the small- $\eta$  limit,  $\boldsymbol{\eta} = 2\boldsymbol{\gamma}$ .

Consider the second moment tensor of an infinitely thin disk inclined by an angle  $\theta$ , with azimuthal angle  $\phi = 0$ . Normalizing this tensor to unit determinant, we obtain

$$\frac{I_{ij}}{|\mathbf{I}|} = \begin{pmatrix} 1/\cos \theta & 0 \\ 0 & \cos \theta \end{pmatrix} = S_{\boldsymbol{\eta}} \mathbf{1}_2 S_{\boldsymbol{\eta}}^T, \quad (16)$$

where  $\mathbf{1}_2$  is the two-dimensional identity matrix, and we have defined the effective shear  $\boldsymbol{\eta}$  through  $\exp(-\boldsymbol{\eta}) = \cos \theta$  and  $\varphi = 0$ . The relation between  $\eta$  and  $\mu = \cos \theta$  for a thin disk can also be derived by noting that the ellipticity [Eq. (27)] is given by  $e = (1 - \mu^2)/(1 + \mu^2)$  and  $e = \tanh \eta$  (Bernstein and Jarvis 2002). Thus, the image of a disk galaxy oriented by angles  $\theta, \phi$  is given by the action on a face-on disk (circular image) by a shear

$$\boldsymbol{\eta}_{\text{orien}}(\theta, \phi): \quad \exp[-\boldsymbol{\eta}] = \cos \theta; \quad \varphi = \phi. \quad (17)$$

Here we have chosen by convention to make  $\eta$  non-negative; face-on ( $\theta = 0$ ) corresponds to  $\eta = 0$ , while edge-on ( $\theta = \pi/2$ ) corresponds to  $\eta \rightarrow +\infty$ . We can thus perform the complete calculation of rotation/projection and lensing in conformal shear space. For this, we need the composition law of conformal shear, which is *non-commutative*. The sum of two shears is given by the unique symmetric unit-determinant matrix which is



equal to the composition of the two shear matrices modulo a rotation (Bernstein and Jarvis 2002). This yields

$$\begin{aligned}\boldsymbol{\eta} &= \boldsymbol{\eta}_1 \oplus \boldsymbol{\eta}_2 : \\ \cosh \eta &= \cosh \eta_1 \cosh \eta_2 + \sinh \eta_1 \sinh \eta_2 \cos(2[\varphi_1 - \varphi_2]) \\ \sinh \eta \sin(2[\varphi - \varphi_1]) &= \sinh \eta_2 \sin(2[\varphi_2 - \varphi_1]).\end{aligned}\quad (18)$$

We now turn to Eq. (14), written in terms of the conformal shear for the time being. We replace the moment tensor on the sky  $\hat{I}_{\text{sky}}$  with the shear  $\hat{\boldsymbol{\eta}}$  estimated using standard techniques from the second moments. Using Bayes' theorem, the posterior is given by

$$\begin{aligned}P(\boldsymbol{\eta}|\hat{\Delta\mathbf{x}}, \hat{\boldsymbol{\eta}}) &= \frac{1}{\mathcal{N}} P(\hat{\Delta\mathbf{x}}, \hat{\boldsymbol{\eta}}|\boldsymbol{\eta}) P(\boldsymbol{\eta}) \\ &= \frac{1}{\mathcal{N}} P(\boldsymbol{\eta}) \int_0^1 d\cos\theta \int_0^{2\pi} d\phi P(\hat{\Delta\mathbf{x}}, \hat{\boldsymbol{\eta}}|\boldsymbol{\eta}, \theta, \phi),\end{aligned}\quad (19)$$

where  $\mathcal{N}$  is a normalization constant and  $P(\boldsymbol{\eta})$  is the prior probability of the shear  $\boldsymbol{\eta}$  (we assume that there is a flat prior on the angle of the shear).  $P(\hat{\Delta\mathbf{x}}, \hat{\boldsymbol{\eta}}|\boldsymbol{\eta}, \theta, \phi)$  is the probability of obtaining a centroid shift and shear as measured ( $\hat{\Delta\mathbf{x}}$  and  $\hat{\boldsymbol{\eta}}$ , respectively), *given true* shear vector  $\boldsymbol{\eta}$  and orientation angles  $\theta, \phi$ . We now transform the integral over orientation angles  $\theta$  to shear  $\boldsymbol{\eta}_d$ , through Eq. (17):

$$\begin{aligned}P(\boldsymbol{\eta}|\hat{\Delta\mathbf{x}}, \hat{\boldsymbol{\eta}}) &= \frac{P(\boldsymbol{\eta})}{\mathcal{N}'} \int_0^\infty e^{-\eta_d} d\eta_d \int_0^{2\pi} d\phi_d P(\hat{\Delta\mathbf{x}}, \hat{\boldsymbol{\eta}}|\boldsymbol{\eta}, \boldsymbol{\eta}_d) \\ &= \frac{P(\boldsymbol{\eta})}{\mathcal{N}'} \int_0^\infty e^{-\eta_d} d\eta_d \int_0^{2\pi} d\phi_d P(\hat{\Delta\mathbf{x}}|\boldsymbol{\eta}_d) P(\hat{\boldsymbol{\eta}}|\boldsymbol{\eta}, \boldsymbol{\eta}_d).\end{aligned}\quad (20)$$

In the second line we have used that the probability factorizes into one for the centroid shift, which only depends on the orientation  $\boldsymbol{\eta}_d$ , and a second factor for the shear estimate. We assume a Gaussian error on  $\hat{\Delta\mathbf{x}}$ , so that

$$P(\hat{\Delta\mathbf{x}}|\boldsymbol{\eta}_d) = N_2 \left[ \hat{\Delta\mathbf{x}} - \Delta\mathbf{x}_{\text{true}}(\boldsymbol{\eta}_d), \sigma_{\Delta\mathbf{x}} \right]. \quad (21)$$

Here,  $N_2$  denotes the bivariate normal distribution and  $\sigma_{\Delta\mathbf{x}}$  is the square root of the variance of each component of  $\Delta\mathbf{x}$  [given by the observational error on the centroid shift, in our case Eq. (13)]. Further,  $\Delta\mathbf{x}_{\text{true}}(\boldsymbol{\eta}_d)$  denotes the true (mean) centroid shift of a galaxy oriented by  $\theta, \phi$  related to  $\boldsymbol{\eta}_d$  through Eq. (17). On the other hand, we neglect observational errors on the second moments of the galaxy image, so that

$$P(\hat{\boldsymbol{\eta}}|\boldsymbol{\eta}, \boldsymbol{\eta}_d) = \delta_D^{(2)}[\hat{\boldsymbol{\eta}} \ominus (\boldsymbol{\eta} \oplus \boldsymbol{\eta}_d)]. \quad (22)$$

That is, the shear estimated from the observed second moments is exactly equal to the shear-space composition of the orientation  $\boldsymbol{\eta}_d$  and the assumed lensing shear  $\boldsymbol{\eta}$ . Of course, these do not in general have the same azimuthal angle. It is straightforward to generalize Eq. (22) to allow for a finite uncertainty in the shear estimate  $\hat{\boldsymbol{\eta}}$ .

Performing the integral over  $\boldsymbol{\eta}_d$  straightforwardly yields

$$\begin{aligned}P(\boldsymbol{\eta}|\hat{\Delta\mathbf{x}}, \hat{\boldsymbol{\eta}}) &= \frac{1}{\mathcal{N}'} P(\boldsymbol{\eta}) \\ &\times \left\{ e^{-\eta_d} N_2 \left[ \hat{\Delta\mathbf{x}} - \Delta\mathbf{x}_{\text{true}}(\boldsymbol{\eta}_d), \sigma_{\Delta\mathbf{x}} \right] \right\}_{\boldsymbol{\eta}_d = \hat{\boldsymbol{\eta}} \ominus \boldsymbol{\eta}}.\end{aligned}\quad (23)$$

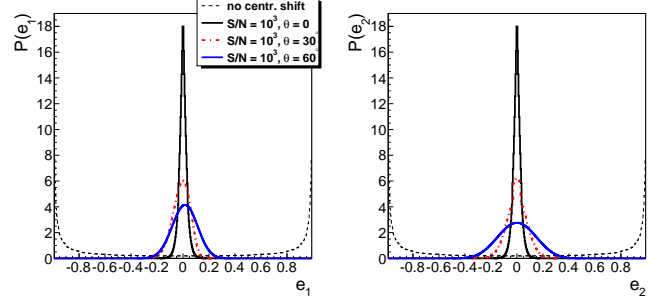


**Figure 5.** Marginalized posterior for the ellipticity components  $e_1, e_2$  for  $\nu = 1000$  and different inclination angles  $\theta$ . In our coordinate convention ( $\varphi = 0$ ),  $e_2$  is the component unaffected by the inclination angle. The thin black line shows the posterior without any orientation information, equivalent to letting  $\nu \rightarrow 0$  in our calculation.

If there is no information on the centroid shift (equivalent to taking  $\sigma_{\Delta\mathbf{x}} \rightarrow \infty$ ), and we assume a flat prior, then

$$P(\boldsymbol{\eta}|\hat{\Delta\mathbf{x}}, \hat{\boldsymbol{\eta}}) \propto \cos\theta(\boldsymbol{\eta}, \hat{\boldsymbol{\eta}}), \quad (24)$$

where  $\theta(\boldsymbol{\eta}, \hat{\boldsymbol{\eta}})$  is the orientation angle of a galaxy that, when lensed by  $\boldsymbol{\eta}$ , yields moments  $\hat{\boldsymbol{\eta}}$ . This is the expected PDF of shape noise for perfect circular disks.

For our studies,  $\hat{\boldsymbol{\eta}}$  will be assumed to correspond to a disk oriented by some fixed fiducial angles  $\theta_0, \phi_0$  (that is, we assume no lensing), and we will let  $\phi_0 = 0$  without loss of generality. We then define  $\boldsymbol{\eta}_0$  through  $\exp(-\boldsymbol{\eta}_0) = \cos\theta_0$ . Further, let  $\varphi$  denote the azimuthal angle of  $\boldsymbol{\eta}$ . Then,  $-\boldsymbol{\eta}$  has azimuthal angle  $\varphi + \pi/2$  (a sign flip in the shear corresponds to rotation by 90 degrees). We then obtain

$$\begin{aligned}\boldsymbol{\eta}_d &= \hat{\boldsymbol{\eta}} \oplus (-\boldsymbol{\eta}) \quad \Leftrightarrow \\ \cosh \eta_d &= \cosh \eta_0 \cosh \eta - \sinh \eta_0 \sinh \eta \cos(2\varphi) \\ \sin(2\varphi_d) &= -\frac{\sinh \eta}{\sqrt{\cosh^2 \eta_d - 1}} \sin(2\varphi).\end{aligned}\quad (25)$$

Note that  $\varphi = 0$  implies  $\varphi_d = 0$ . This is because the sum of two aligned shears is in the same direction. For  $\varphi \neq 0$ , we pick the solution that connects continuously to  $\varphi = 0 = \varphi_d$ .

In order to solve for  $\theta_d$ , we need to pick a branch of the quadratic solution. This is easily done using  $\cosh \eta_d \geq 1$  and  $\cos\theta_d \in [0, 1]$ . We obtain

$$\cos\theta_d = \cosh \eta_d - \sqrt{\cosh^2 \eta_d - 1}. \quad (26)$$

For a fixed value of  $\theta_0$ , it is then straightforward to map out the posterior Eq. (23) in the  $\boldsymbol{\eta}$  plane.

However, in order to derive the shape noise predicted by this posterior, it is more practical to transform from  $\boldsymbol{\eta}$  to the ellipticity (or distortion)  $\mathbf{e}$ , defined through

$$e_1 = \frac{I_{11} - I_{22}}{\text{Tr } I_{ij}}; \quad e_2 = \frac{2I_{12}}{\text{Tr } I_{ij}}. \quad (27)$$

Note that  $e_i \in [-1, 1]$ , and that at linear order, lensing changes the ellipticity  $\mathbf{e}$  through

$$\mathbf{e} \rightarrow \mathbf{e} + 2\boldsymbol{\gamma} \quad (28)$$

where  $\boldsymbol{\gamma}$  is the shear vector. Following Eq. (2.7) of Bern-

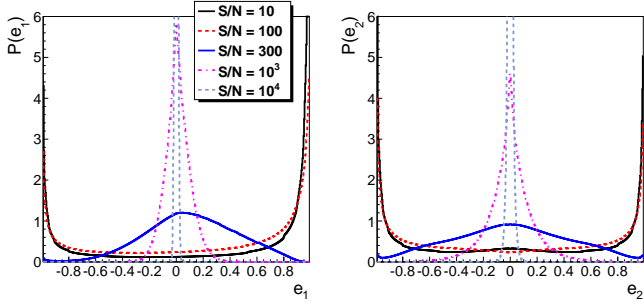


**Figure 6.** Marginalized posterior for the ellipticity components  $e_1$ ,  $e_2$  averaged over inclination angles for different values of signal-to-noise.

stein and Jarvis (2002),

$$\mathbf{e}(\eta) = \tanh \eta \begin{pmatrix} \cos 2\varphi \\ \sin 2\varphi \end{pmatrix}, \quad (29)$$

where  $\varphi$  is the azimuthal angle of  $\boldsymbol{\eta}$ , so that

$$\begin{aligned} P(\mathbf{e}|\Delta\mathbf{x}, \hat{\boldsymbol{\eta}}) &= P(\boldsymbol{\eta}(\mathbf{e})|\Delta\mathbf{x}, \hat{\boldsymbol{\eta}}) \left| \frac{\partial \boldsymbol{\eta}}{\partial \mathbf{e}} \right| \\ &= P(\boldsymbol{\eta}(\mathbf{e})|\Delta\mathbf{x}, \hat{\boldsymbol{\eta}}) (1 - e^2)^{-2}, \end{aligned} \quad (30)$$

where

$$\eta(e) = \frac{1}{2} \ln \left( \frac{1+e}{1-e} \right). \quad (31)$$

Fig. 5 shows the posterior for the two components  $e_1$ ,  $e_2$  of the residual ellipticity for different true orientation angles at fixed signal-to-noise  $\nu = 1000$ . Clearly, the ellipticity is well constrained, with sharper constraints for smaller inclinations. This is because degeneracies between orientation and lensing increase for finite inclinations. The thin black line shows the posterior if no centroid shift is measured. The posterior is then very broad with a peak at  $e_i \rightarrow \pm 1$ . This is just the consequence of the uniform prior on  $\cos \theta$ .

Fig. 6 shows the posterior for the ellipticity components averaged over inclination angle  $\theta_0$ . The results are shown for different values of the image signal-to-noise. There is a rapid transition between values  $\nu \sim 100$ , up to which the distribution of residual ellipticity is broad, and  $\nu \sim 10^3$ , when the orientation of the galaxy is well constrained and the residual ellipticity follows a narrow distribution centered around zero.

In the end, we would like to estimate the residual shape noise after the centroid shift has been optimally taken into account. This is approximately quantified by the RMS of the posterior for the two ellipticity components, specifically

$$\text{RMS}(e_i) = \left[ \int_{-1}^1 d^2\mathbf{e}(e_i)^2 P(\mathbf{e}|\Delta\mathbf{x}, \hat{\boldsymbol{\eta}}) \right]^{1/2}, \quad (32)$$

where we have used that both components have vanishing expectation value (unlike the magnitude  $|\mathbf{e}|$ ). In order to estimate the residual shape noise, we use the quantity  $\sigma_e$  defined through

$$\sigma_e = \frac{1}{\sqrt{2}} \left( [\text{RMS}(e_1)]^2 + [\text{RMS}(e_2)]^2 \right)^{1/2}, \quad (33)$$

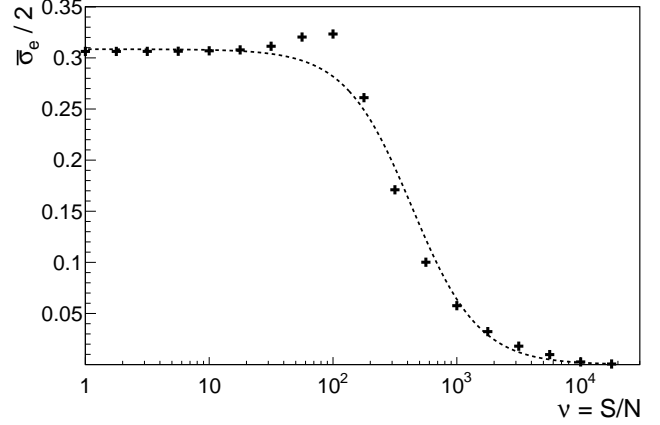


**Figure 7.** RMS ellipticity averaged over  $\theta_0$  following Eq. (34) as function of signal-to-noise. We have divided the RMS by 2 since that gives the shape noise contribution to the RMS of each shear component. The line shows the fit given in Eq. (40).

which is the average noise per component of the ellipticity. As shown in Fig. 5, this quantity depends on the orientation angle of the galaxy. In order to estimate the effective shape noise for an ensemble of galaxies with random orientations, we perform an inverse-variance weighting to obtain

$$\bar{\sigma}_e = \left[ \int_0^1 d \cos \theta_0 \sigma_e^{-2}(\theta_0) \right]^{-1/2}. \quad (34)$$

This is not exactly what one would do in reality, since in practice one has to use the centroid shift and/or shape of the galaxy to estimate  $\theta_0$ . Further, the posterior for  $e_i$  is highly non-Gaussian, especially for small signal-to-noise, so that Eq. (34) is not optimal. However, we take it as a first approximation. The result is shown as function of galaxy signal-to-noise in Fig. 7, where we have divided  $\bar{\sigma}_e$  by two in order to yield the effective shape noise  $\sigma_\gamma$ . It shows the expected behavior: for low signal-to-noise values where the centroid shift is not detectable observationally, the RMS of the residual ellipticity approaches a constant corresponding to the usual shape noise for randomly oriented disk galaxies. Once the centroid shift can be measured, the residual RMS drops rapidly. In the intermediate regime ( $\nu \sim 100$ ), we see that the RMS actually increases for increasing signal-to-noise. This is due to the deficiencies of the simple weighting scheme in Eq. (34); indeed, when performing a uniform weighting over orientation, this feature goes away. Note that for an ellipticity RMS better than 0.1, achieved at signal-to-noise values of order a thousand, we expect departures from a perfect thin disk to become relevant (Ryden 2004).

### 3.1. Impact on shear surveys

We have seen that the centroid shift can significantly reduce the residual shape noise for disk galaxies at high signal-to-noise. In the following, we will use

$$\sigma_{\text{int, res}} = \frac{1}{2} \bar{\sigma}_e \quad (35)$$

as estimate for the residual shape noise, i.e. the RMS in each component of the shear, where the factor of 1/2

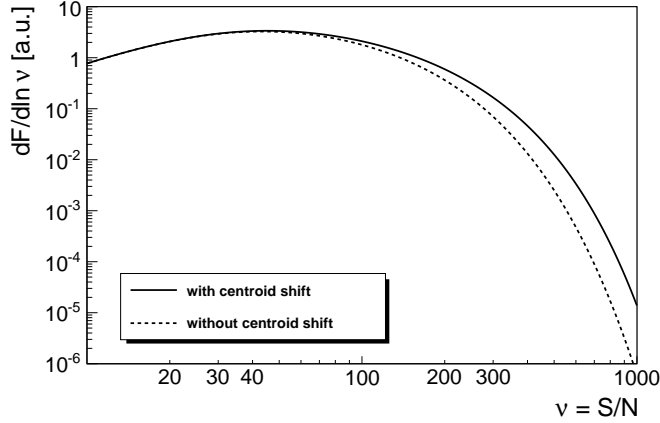


**Figure 8.** Information content of galaxies for shear estimation per logarithmic interval in signal-to-noise  $\nu$  without (dashed) and with (solid) using the centroid shift.

comes from Eq. (28). The question then arises to what extent this reduces the noise overall in shear surveys. Note that this reduction only applies to disk galaxies, which make up the majority of but not all galaxies in imaging surveys. Thus, when we talk about the number density of galaxies in the following we will always mean the number density of disk galaxies. In order to estimate the reduction in noise, we define the Fisher information delivered by galaxies within a logarithmic interval in the signal-to-noise  $\nu$ :

$$\frac{dF}{d \ln \nu} = \frac{dn_g}{d \ln \nu} \sigma_\gamma^{-2}(\nu), \quad (36)$$

where  $dn_g/d \ln \nu$  is the number density of source galaxies per logarithmic  $\nu$  interval, and  $\sigma_\gamma$  is the effective shape noise for galaxies of signal-to-noise  $\nu$ . At fixed redshift,  $dn_g/d \ln \nu$  roughly follows a Schechter function, i.e. it drops exponentially at high  $\nu$ . On the other hand, when averaged over a wide redshift range,  $dn_g/d \ln \nu$  approaches a power law. Samples selected for lensing measurements typically use a cut on photometric redshift to exclude low-redshift galaxies which do not contribute to the lensing measurement. For this reason, we will assume an exponential distribution,

$$\frac{dn_g}{d \ln \nu} \propto \exp\left(-\frac{\nu}{\nu_*}\right), \quad (37)$$

up to a normalization constant which is irrelevant here. This choice is conservative, as it reduces the number of very high signal-to-noise galaxies as compared to a power law distribution. We have used the weak lensing shear sample of the COSMOS survey (Leauthaud et al. 2007) to confirm that  $\nu_* \approx 60$  roughly describes the signal-to-noise distribution for photometric redshifts  $z \in [0.5, 1.5]$  (note that the values of  $\nu$  in the catalog are only approximate, since they neglect pixel-level noise correlations).

For the shape noise, we assume

$$\sigma_\gamma^2(\nu) = \sigma_{\text{meas}}^2(\nu) + \sigma_{\text{int, res}}^2(\nu), \quad (38)$$

where  $\sigma_{\text{meas}}$  is the contribution from measurement errors in the galaxy shape, while  $\sigma_{\text{int, res}}$  is the residual shape noise due to the imperfect measurement of the centroid shift and resulting uncertainty in the orientation. The

latter is calculated from the results of the previous section through Eq. (35). We assume that  $\sigma_{\text{meas}}$  is inversely proportional to  $\nu$ , specifically

$$\sigma_{\text{meas}}(\nu) = \frac{\nu_0}{\nu}, \quad (39)$$

and we adopt  $\nu_0 = 10$  as fiducial value. The scaling with  $\nu^{-1}$  has been found to roughly describe the uncertainty of the image second moments in the simulations of Massey et al. (2007) (App. C). The value of  $\nu_0$  was simply chosen to yield a typical noise level expected in shear samples involving a signal-to-noise threshold of 20–40. For convenience, we parametrize  $\sigma_{\text{int, res}}$  through

$$\sigma_{\text{int, res}}(\nu) = 0.31 \frac{(\nu/\nu_r)^{-p}}{1 + (\nu/\nu_r)^{-p}}, \quad \nu_r \approx 433, \quad p \approx 1.6, \quad (40)$$

which provides a reasonable fit (see Fig. 7). The results are shown in Fig. 8. The centroid shift significantly increases the information content of high-signal-to-noise galaxies. For the fiducial values chosen here, it does not significantly increase the total information on weak lensing shear, given by the integral under the curves in Fig. 8, which is dominated by galaxies with  $20 \lesssim \nu \lesssim 100$ . This conclusion however depends strongly on the amplitude of the centroid shift. A centroid shift greater by a factor of two, which could be possible in imaging surveys due to larger optical depth of galaxies at higher redshift, already yields a significant enhancement in the total information. Finally, these results also depend on the precise high- $\nu$  tail of the signal-to-noise distribution of galaxies, which will not be exactly exponential.

Note that for sufficiently high  $\nu$ , one should take into account the noise from the fact that galaxy disks are not perfectly circular. However, this will only become important for  $\nu \gtrsim 10^3$ . One important caveat is that we have assumed that the centroid shift is only a function of inclination, and neglected scatter in the dust content and scale height ratios from galaxy to galaxy. Further investigation, in particular using actual data, is warranted in order to realistically assess the importance of the centroid shift for reducing the shape noise in shear surveys.

#### 4. PROBING THE DUST CONTENT OF DISK GALAXIES

An alternative application of the centroid shift is to use the measurement in conjunction with measured shapes to obtain the optical depth due to dust extinction for a large sample of galaxies. This could be an interesting complement to existing studies of dust content which are typically restricted to fairly small sample sizes.

The approach is the following: we now use the galaxy shape to constrain the orientation of the galaxy, which in turn predicts the centroid shift assuming a value of the optical depth. Comparing this to the measured centroid shift allows us to constrain the optical depth. Let us write the actual centroid shift as

$$\Delta \mathbf{x}_{\text{true}}(\tau, \theta) = \tau \Delta \mathbf{x}_0(\theta), \quad (41)$$

where  $\tau = \tau_{\text{fo}, a} - \tau_{\text{fo}, b}$  is the difference in face-on optical depth between the two bands which are used to measure the centroid shift.  $\Delta \mathbf{x}_0(\theta)$  is assumed to be a universal function, although in reality this will vary from galaxy



to galaxy due to different dust distributions. Our goal is then to construct the posterior for  $\tau$  given a measurement of the centroid shift  $\hat{\Delta}\mathbf{x}$  and second moments on the sky  $\hat{I}_{\text{sky}}$ . As in the previous section, we will parametrize  $\hat{I}_{\text{sky}}$  through the conformal shear vector  $\hat{\eta}$ . Thus, our goal is to calculate  $P(\tau|\hat{\Delta}\mathbf{x}, \hat{\eta})$ . In principle, one should marginalize over the weak lensing shear when estimating the orientation from  $\hat{\eta}$ . However, since the lensing effect is small and we are only interested in a rough estimate, we will assume that there is no lensing; in the framework of the derivation in the previous section, we adopt a prior of  $\delta_D^{(2)}(\eta)$ . This yields

$$\begin{aligned} P(\tau|\hat{\Delta}\mathbf{x}, \hat{\eta}) &= \frac{1}{\mathcal{N}} P(\hat{\Delta}\mathbf{x}, \hat{\eta}|\tau) P(\tau) \\ &= \frac{P(\tau)}{\mathcal{N}} \int d\cos\theta \int d\phi P(\hat{\Delta}\mathbf{x}, \hat{\eta}|\tau, \theta, \phi), \end{aligned}$$

where  $\mathcal{N}$  is a normalization constant,  $P(\tau)$  is the prior on  $\tau$ , and  $\theta, \phi$  are the true orientation angles of the galaxy. As before, we neglect the uncertainty on  $\hat{\eta}$ , assuming that the second moments are very well measured, and adopt a Gaussian distribution for the observed centroid shift. This yields

$$\begin{aligned} P(\tau|\hat{\Delta}\mathbf{x}, \hat{\eta}) &= \frac{1}{\mathcal{N}'} P(\tau) \\ &\times \left\{ e^{-\eta} N_2 \left[ \hat{\Delta}\mathbf{x} - \Delta\mathbf{x}_{\text{true}}(\tau, \eta), \sigma_{\Delta\mathbf{x}} \right] \right\}_{\eta=\hat{\eta}}. \end{aligned} \quad (42)$$

Let us assume that the expectation value of  $\hat{\Delta}\mathbf{x}$  is  $\Delta\mathbf{x}_{\text{true}}(\tau_{\text{true}}, \eta_{\text{true}})$ , where  $\tau_{\text{true}}$  is the actual optical depth. One can easily see that Eq. (42) becomes

$$P(\tau|\hat{\Delta}\mathbf{x}, \hat{\eta}) = \frac{1}{\mathcal{N}''} P(\tau) \cos\theta \quad (43)$$

$$\times \exp \left[ - \left( \frac{\Delta\mathbf{x}_0(\theta)}{\sigma_{\Delta\mathbf{x}}} \right)^2 (\tau - \tau_{\text{true}})^2 \right], \quad (44)$$

where  $\theta$  is the orientation angle estimated from  $\hat{\eta}$ , which under our assumptions is the true orientation angle. Thus, at fixed orientation angle the optical depth is Gaussian-distributed with RMS

$$\text{RMS}(\tau) = \frac{\sigma_{\Delta\mathbf{x}}}{\Delta\mathbf{x}_0(\theta)}. \quad (45)$$

In particular, for  $\theta \rightarrow 0$  the variance becomes infinite, since the centroid shift vanishes for any  $\tau$ . This is illustrated in Fig. 9, where we show the posterior for  $\tau$  at fixed signal-to-noise for different values of  $\theta$ .

We can now perform an inverse-variance weighting over orientation angles, in analogy with Eq. (34). The result can be simply cast into the form

$$\bar{\sigma}_\tau = 0.29 \left( \frac{\nu}{100} \right)^{-1}. \quad (46)$$

For galaxies with signal-to-noise greater than a few hundred,  $\tau$  can thus be measured very accurately. In order to roughly estimate the number density of galaxies in state-of-the-art imaging surveys such as CFHTLenS (Heymans et al. 2012), DES (The Dark Energy Survey Collaboration 2005), or HSC (Miyazaki et al. 2012) that will yield dust estimates through centroid shift measurements, we

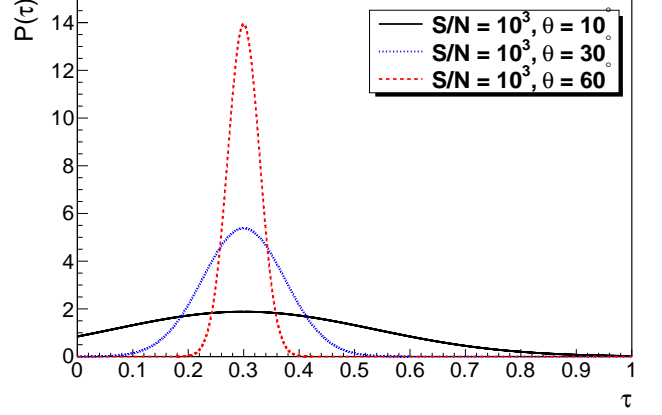


**Figure 9.** Posterior for the relative face-on optical depth between bands from which the centroid shift is measured, for  $\nu = 1000$  and different inclination angles  $\theta$ . Our fiducial choice is  $\tau_{\text{true}} = 0.3$ . Note that for  $\theta \rightarrow 0$ , there is no constraint on the optical depth.

assume a number density of  $\sim 10 \text{ arcmin}^{-2}$  above  $\nu \sim 20$ , which leads to an estimate of  $\sim 0.1 \text{ arcmin}^{-2}$  for galaxies with  $\nu \gtrsim 200$  using our exponential ansatz in Eq. (37). This corresponds to 360 galaxies per square degree with detectable centroid shift. Taking into account the considerable uncertainties in this measurement, an expectation of several hundred galaxies per square degree seems reasonable, which, for surveys covering thousands of square degrees, yields dust extinction estimates for several hundred thousand galaxies.

## 5. CONCLUSIONS

We have shown that dust extinction leads to a shift of the centroid of galaxy images in different bands, focusing in particular on disk galaxies. This shift is a well-defined function of inclination of the disk, with amplitude mainly determined by the intrinsic, face-on optical depth in each band, and the relative scale heights and lengths of opacity and emissivity in the galaxy. We estimated that this centroid shift should be detectable for galaxies with signal-to-noise values greater than of order 100. In state-of-the-art imaging surveys, this translates to number densities of several hundred galaxies per square degree with measurable centroid shift. This centroid shift could be interesting for two purposes.

First, given independent (statistical) constraints on the dust optical depth, the centroid shift can be used to infer galaxy orientations. The unknown orientation is the main reason for non-circular apparent shapes of disk galaxies, and thus the main source of shape noise in weak lensing shear surveys. For high signal-to-noise galaxies, the centroid shift can thus reduce shape noise and significantly increase their importance for estimating shear. We have found that for our fiducial assumptions about typical optical depths, the increase in overall information on shear is modest. However, should dust extinction increase towards higher redshift (where most source galaxies in shear surveys reside), then this approach could yield a significant increase in lensing information extractable from imaging surveys. A caveat to this is that we have not included scatter in optical depth and scale height ratios which determine the normalization of the centroid shift-inclination relation for a given

galaxy. We believe however that this application of the centroid shift warrants further study.

A complementary application of this effect is to neglect lensing and use the observed galaxy shapes as a measure of their orientation. Then, the centroid shift is a new, independent probe of dust extinction which is directly applicable to a large number of galaxies (we have estimated hundreds of thousands of galaxies in state-of-the-art imaging surveys). Together with modeling of galaxy SEDs, this should provide crucial constraints breaking some of the degeneracies present in dust modeling, e.g. the distribution of dust and orientation.

Finally, and perhaps most importantly, one of the first steps should be to look for this effect in existing data. Our estimates show that it should easily be detectable in currently available samples such as from SDSS or CFTHLenS.

*Acknowledgments:* We would like to thank Jim Bosch, Bruce Draine, Simone Ferraro, Brandon Hensley, Eric Huff, Guinevere Kauffmann, Alexie Leauthaud, Robert Lupton, Rachel Mandelbaum, Richard Massey, Hironao Miyatake, David Spergel and Michael Strauss for helpful discussions and comments.

## APPENDIX

### A. ANALYTICAL ESTIMATE OF CENTROID OFFSET

In this appendix we derive an analytical solution to Eq. (4) in the limit that  $z_{\text{gf}} \tan \theta / r_{\text{gf}}$  is a small parameter. This limit assumes that the radial distance traveled by the light ray while within the region where  $\epsilon$  and  $\kappa$  are non-negligible is much smaller than the radial distance at which it originated. Clearly, this condition can be satisfied by making  $\theta$  sufficiently small, but it can also be satisfied at finite  $\theta$  when the disk scale height of the galaxy is much smaller than its scale length, since the integrand in Eq. (4) is then only relevant for  $|z_{\text{gf}}| \ll r_{\text{gf}}$ . Conversely, for sufficiently large inclinations  $\theta$  this expansion will break down.

Throughout we will work in galaxy-frame cylindrical coordinates  $r_{\text{gf}}, \varphi_{\text{gf}}, z_{\text{gf}}$ , and for clarity we will drop the subscript “gf” in the remainder of this appendix. We expand Eq. (4) to linear order in  $z \tan \theta / r$ , yielding

$$I_{\text{obs}}(r, \varphi; \theta) = \frac{1}{\cos \theta} [I_0(r; \theta) + \cos \varphi I_1(r; \theta)] \quad (\text{A1})$$

where we have defined

$$I_0(r; \theta) = \int_{-\infty}^{\infty} dz \epsilon(r, z) \exp \left[ -\frac{1}{\cos \theta} \int_z^{\infty} \kappa(r, z') dz' \right] \quad (\text{A2})$$

$$I_1(r; \theta) = \tan \theta \int_{-\infty}^{\infty} dz \left[ z \frac{\partial \epsilon(r, z)}{\partial r} - \frac{\epsilon(r, z)}{\cos \theta} \int_z^{\infty} dz' z' \frac{\partial \kappa(r, z')}{\partial r} \right] \exp \left[ -\frac{1}{\cos \theta} \int_z^{\infty} \kappa(r, z') dz' \right]. \quad (\text{A3})$$

$I_0$  is the leading order intensity distribution of the galaxy in this expansion, which is independent of  $\varphi$  and hence does not show a centroid shift. The centroid shift is induced by the second term, Eq. (A3), which is proportional to  $\cos \varphi$ . We define the centroid of the observed intensity  $\mathbf{x}_c$  through,

$$\mathbf{x}_c = \left[ \int r dr w(r) \int d\varphi I_{\text{obs}} \right]^{-1} \int_0^{\infty} r dr w(r) \int_0^{2\pi} d\varphi \begin{pmatrix} r \cos \varphi \\ r \sin \varphi \end{pmatrix} I_{\text{obs}}(r, \varphi; \theta), \quad (\text{A4})$$

where we have allowed for a weighting function  $w(r)$  (see App. B). Eqs. (A2)–(A3) then immediately yield at leading order

$$x_c^1 = \frac{1}{2} \left[ \int r dr w(r) I_0(r; \theta) \right]^{-1} \int_0^{\infty} r^2 dr w(r) I_1(r; \theta); \quad x_c^2 = 0. \quad (\text{A5})$$

As expected, the centroid shift is aligned with the  $x$  axis for the coordinate system adopted. We thus need to estimate the relative magnitudes of  $I_1(r; \theta)$  and  $I_0(r; \theta)$ .

We can make the expressions more transparent by defining the face-on integrated opacity or “partial optical depth”  $\tau_{\text{fo}}(r, z) = \int_z^{\infty} dz' \kappa(r, z')$  and the scale lengths

$$r_{\epsilon}^{-1}(r) \equiv -\frac{\partial \ln \epsilon(r, z \simeq 0)}{\partial r}; \quad r_{\kappa}^{-1}(r) \equiv -\frac{\partial \ln \kappa(r, z \simeq 0)}{\partial r}, \quad (\text{A6})$$

which are positive if emissivity and opacity increase towards the center of the galaxy. Further, we define an effective scale height for the emissivity  $\hat{z}_{\epsilon}$  through

$$\hat{z}_{\epsilon}(r; \theta) \equiv \frac{1}{I_0(r; \theta)} \int_{-\infty}^{\infty} dz z \epsilon(r, z) e^{-\tau_{\text{fo}}(r, z) / \cos \theta}. \quad (\text{A7})$$

Note that (for a galaxy symmetric under  $z \rightarrow -z$ )  $\hat{z}_\epsilon$  vanishes unless  $\tau_{\text{fo}} \neq 0$ . Similarly, we define an effective opacity scale height,

$$\hat{z}_\kappa(r; \theta) \equiv \frac{1}{I_0(r; \theta) \cos \theta} \int_{-\infty}^{\infty} dz \epsilon(r, z) e^{-\tau_{\text{fo}}(r, z) / \cos \theta} \int_z^{\infty} dz' z' \kappa(r, z'). \quad (\text{A8})$$

In the following, we will omit the  $r$  and  $\theta$  dependence of  $r_\epsilon$ ,  $r_\kappa$ ,  $\hat{z}_\epsilon$ ,  $\hat{z}_\kappa$  for clarity. At leading order, we then have

$$\frac{I_1(r; \theta)}{I_0(r; \theta)} = \tan \theta \left( \frac{\hat{z}_\kappa}{r_\kappa} - \frac{\hat{z}_\epsilon}{r_\epsilon} \right). \quad (\text{A9})$$

From Eq. (A5) we see that, modulo a radial weighting, this ratio determines the fractional centroid shift.

As an example, consider the case where the emissivity is located at  $z = 0$ , while the absorbing material (dust) follows a more extended distribution, with  $r_\epsilon \sim r_\kappa$ . Then,  $\hat{z}_\epsilon \ll \hat{z}_\kappa$ . Thus, Eq. (A9) becomes

$$\frac{I_1(r; \theta)}{I_0(r; \theta)} = \tan \theta \frac{\hat{z}_\kappa}{r_\kappa}. \quad (\text{A10})$$

This says that the half of the galaxy closer to the observer ( $x > 0$ ) suffers less absorption than the other half further away. In the opposite case, where a distribution of emissivity surrounds a dust screen at  $z = 0$ , we have

$$\frac{I_1(r; \theta)}{I_0(r; \theta)} = -\tan \theta \frac{\hat{z}_\epsilon}{r_\epsilon}. \quad (\text{A11})$$

In this case, more emissivity contributes on the side of the galaxy that is further away from the observer, leading to a centroid shift in the negative  $x$  direction. In general some cancellation can occur between the two competing effects, although note that the effect will be non-zero for an identical distribution of  $\epsilon$  and  $\kappa$  due to the different weighting involved in  $\hat{z}_\epsilon$  and  $\hat{z}_\kappa$  (unless of course both  $\hat{z}_\epsilon$  and  $\hat{z}_\kappa$  vanish). We thus already see the two main factors which determine the centroid shift: the optical depth  $\tau \propto \int dz \kappa$ , and the ratio  $z/r$  of typical scale height to scale length of the galaxy.

We can now specialize to the case of an exponential disk, Eq. (7). For simplicity, we will also linearize the result in  $\tau_{\text{fo}}$ , which given  $\tau_{\text{fo}} \sim 0.2 - 0.5$  is sufficiently accurate for this approximate estimate. Defining the ratio  $c_z = z_\kappa / z_\epsilon$  of opacity to emissivity scale heights, we obtain

$$\hat{z}_\epsilon = \frac{\tau_{\text{fo}}(r)}{\cos \theta} \frac{1 + 2c_z}{(1 + c_z)^3} z_\epsilon; \quad \hat{z}_\kappa = \frac{\tau_{\text{fo}}(r)}{\cos \theta} \frac{c_z^2(2 + c_z)}{(1 + c_z)^2} z_\epsilon, \quad (\text{A12})$$

which using Eq. (A9) yields

$$\frac{I_1(r; \theta)}{I_0(r; \theta)} = \tan \theta \tau_{\text{fo}}(r) \left[ \frac{r_\epsilon}{r_\kappa} \frac{c_z^2(2 + c_z)}{(1 + c_z)^2} - \frac{1 + 2c_z}{(1 + c_z)^3} \right] \frac{z_\epsilon}{r_\epsilon}. \quad (\text{A13})$$

Here we have dropped a  $1/\cos \theta$  factor which converts the face-on opacity to the actual observed opacity, since this is 1 at leading order in our expansion in  $\tan \theta$ .

Finally, performing the radial weighting in Eq. (A5), we obtain

$$\frac{|\mathbf{x}_c|}{r_w} = \frac{|x_c^1|}{r_w} = \frac{1}{2} \tan \theta \left( \frac{\langle \hat{z}_\kappa \rangle_{rw}}{r_\kappa} - \frac{\langle \hat{z}_\epsilon \rangle_{rw}}{r_\epsilon} \right), \quad (\text{A14})$$

where the weighted effective radius of the galaxy is

$$r_w = \left[ \int r dr w(r) I_0(r; \theta) \right]^{-1} \int_0^\infty r^2 dr w(r) I_0(r; \theta), \quad (\text{A15})$$

and the radial weighting of the scale heights is defined through

$$\langle f(r) \rangle_{rw} \equiv \left[ \int r^2 dr w(r) I_0(r; \theta) \right]^{-1} \int r^2 dr w(r) f(r) I_0(r; \theta). \quad (\text{A16})$$

Using the results for the exponential disk Eq. (A12), this simply becomes

$$\frac{|\mathbf{x}_c|}{r_w} = \frac{1}{2} \tan \theta \langle \tau_{\text{fo}} \rangle_{rw} \left[ \frac{r_\epsilon}{r_\kappa} \frac{c_z^2(2 + c_z)}{(1 + c_z)^2} - \frac{1 + 2c_z}{(1 + c_z)^3} \right] \frac{z_\epsilon}{r_\epsilon}, \quad (\text{A17})$$

which involves the radially weighted face-on optical depth. Inserting the parameters from Eq. (8), this becomes

$$\frac{|\mathbf{x}_c|}{r_w} \simeq 0.04 \tan \theta \langle \tau_{\text{fo}} \rangle_{rw}. \quad (\text{A18})$$

This result explains both the behavior with inclination angle of the centroid shift determined using the radiative transfer calculation as well as the fact that the centroid shift is largest in the innermost regions: choosing a weighting function  $w(r) = \Theta(r_{\max} - r)$  which only includes the regions  $r < r_{\max}$ , we see that  $\langle \tau_{\text{fo}} \rangle_{rw}$  will decrease with increasing  $r_{\max}$ , matching the trend seen in Fig. 3.

For this paper, we adopt a weighting function corresponding to  $r_{\max} = r_{\text{eff}}/2$ . In terms of the literature value  $\tau_{\text{fo}}$ , we then have  $\langle \tau_{\text{fo}} \rangle_{rw} \approx 1.6\tau_{\text{fo}}$  from the radiative transfer results, while  $r_w \approx r_{\text{eff}}$ , which leads to

$$\frac{|\mathbf{x}_c|}{r_{\text{eff}}} \simeq 0.06 \tan \theta \tau_{\text{fo}}. \quad (\text{A19})$$

As a final note, we point out that dust extinction also modifies the galaxy's observed second moments, i.e. its shape. However, this effect is suppressed by another power of the small parameter  $z \tan \theta / r$ , and hence less likely to be detectable than the centroid shift.

## B. OPTIMAL ESTIMATION OF CENTROID OFFSET

Fig. 3 shows that the centroid shift due to dust extinction is not uniform over the galaxy image, but rather is most prominent in the inner regions. For this reason, we derive an approximation to the optimal estimation of the image centroid for the purpose of measuring the extinction-induced centroid offset. Throughout we neglect point-spread-function effects, i.e. we assume that the galaxy is perfectly resolved.

Let us divide the galaxy image into approximately elliptical contours of constant surface brightness (isophotes). A general weighted estimate of the centroid of the galaxy image is then given by

$$\mathbf{x}_w = \frac{\sum_{\text{pixels}} w(\mathbf{x}_i) \mathbf{x}_i}{\sum_{\text{pixels}} w(\mathbf{x}_i)} = \frac{\int r dr w(r) \mu(r) \int_0^\pi d\phi \mathbf{x}(r, \phi)}{\pi \int r dr w(r) \mu(r)}, \quad (\text{B1})$$

where  $\mu(r)$  is the surface brightness, and in the second equality we have gone to the continuum limit and elliptical coordinates parametrized through  $(r, \phi)$ . Our goal is to derive the weight function  $w(\mu)$  that optimally captures the centroid shift.

At fixed inclination  $\theta$ , we can write for the centroid shift of a single isophote  $r$ :

$$\Delta \mathbf{x}(r) = f(\mu(r)) \tau_{\text{fo}}. \quad (\text{B2})$$

The optimal estimate for the centroid shift is then given by the optimal estimate for  $\tau_{\text{fo}}$ . Let  $\mathbf{x}_c(r)$  denote the centroid of the isophote  $r$ , and  $\sigma_{\mathbf{x}_c}(r)$  denote its error. Assuming that the errors from different isophotes are independent, the optimal estimate for  $\tau_{\text{fo}}$  is the inverse-variance weighted average of isophotes:

$$\hat{\tau}_{\text{fo}} = N \int dr \frac{f^2(\mu) \mathbf{x}_c(r)}{\sigma_{\mathbf{x}_c}^2(r) f(\mu)}, \quad (\text{B3})$$

where  $N$  is a normalization constant. Thus, the desired weighting function is given by

$$w(r) = \frac{f(\mu)}{\sigma_{\mathbf{x}_c}^2(r)}. \quad (\text{B4})$$

We now need to estimate the error  $\sigma_{\mathbf{x}_c}$ , specifically its scaling with  $r$ . Following the results of App. C, we assume that

$$\frac{\sigma_{\mathbf{x}_c}(r)}{\max(r, r_{\text{PSF}})} \propto \nu^{-1} \propto \mu^{-1}(r), \quad (\text{B5})$$

where we have assumed that the signal-to-noise  $\nu$  of the elliptical annulus is proportional to its surface brightness. Clearly, this is only a rough approximation, but sufficient for our desired purpose. We then obtain

$$w(r) = \frac{f(\mu(r)) \mu^2(r)}{\max(r^2, r_{\text{PSF}}^2)}. \quad (\text{B6})$$

Fig. 3 shows that  $f(\mu)$  can roughly be approximated as  $\propto \mu^2$ . In this case,  $w(r) \propto \mu^4(r)/\max(r^2, r_{\text{PSF}}^2)$ , which for an exponential profile is very strongly peaked at small radii. Thus, for galaxies at cosmological redshifts the centroid estimate will be dominated by the innermost resolved scales, i.e.  $r \lesssim r_{\text{PSF}}$ .

## C. ESTIMATE OF OBSERVATIONAL CENTROID SHIFT UNCERTAINTY

In order to estimate what accuracy the centroid measurement in an imaging survey has, we use image simulations prepared for the Shear Testing Programme (STEP; Massey et al. (2007)). These image simulations were designed to match space-based imaging. However, we expect that the rough scaling derived from these simulations will also describe ground-based imaging as long as the galaxies are well resolved.

We have several realizations of noise for the same galaxy images, and we calculate the quantities

$$\Delta_x = \frac{x_{c,1} - x_{c,2}}{d}; \quad \Delta_y = \frac{y_{c,1} - y_{c,2}}{d}, \quad (\text{C1})$$

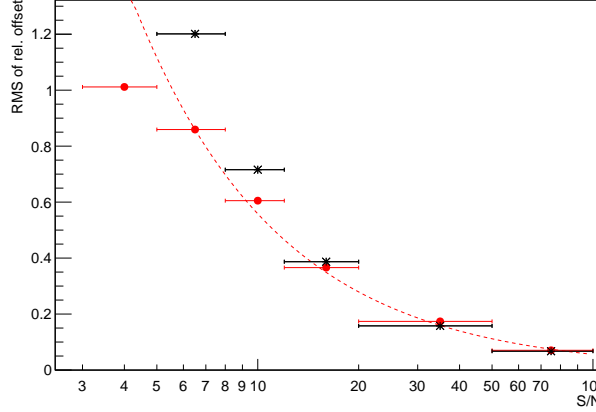


**Figure 10.** RMS scatter in the relative centroid defined in Eq. (C1) as a function of galaxy signal-to-noise, for two different samples of galaxies: those smaller than the median size (red, circles), and larger (black, stars). The dashed line indicates a simple  $1/x$  fit.

where  $x_{c,i}$  correspond to the  $x$ -component of the centroid measured in noise realization  $i$ , and analogously for  $y$ . Here,  $d$  is the weighted size following Rhodes et al. (2000). This is typically  $\sim 0.6$  times the half-light radius. We then calculate the RMS values of  $\Delta_x$  and  $\Delta_y$  and average them in quadrature (the mean has been found to be consistent with zero, as expected). This exercise can be done for various subsamples of the set of simulated galaxy images. Note that the scatter in  $\Delta_x$ ,  $\Delta_y$  necessarily includes some contribution from the scatter in galaxy sizes between different noise realizations. We use the size averaged over noise realizations to reduce this effect, but note that our estimates of the centroid uncertainty will be conservative in this respect.

We have found that the relative offset defined through Eq. (C1) is quite insensitive to galaxy properties and mainly depends on the signal-to-noise  $\nu$  (while the absolute offset strongly depends on the size of the image in addition to the signal-to-noise). This is illustrated in Fig. 10, which shows the RMS of  $\Delta_x$ ,  $\Delta_y$  as function of galaxy signal-to-noise, for two subsamples of different size. There is some indication that larger galaxies have larger scatter in the relative centroid at fixed signal-to-noise, although the effect is not very large. The dashed line indicates a simple fit to the result for the smaller size sample:

$$\text{RMS}(\Delta_{x,y}) = \frac{5.6}{\nu}, \quad (\text{C2})$$

which translates to

$$\text{RMS} \left( \frac{x_c, y_c}{r_{\text{eff}}} \right) = \frac{3.3}{\nu}, \quad (\text{C3})$$

where  $r_{\text{eff}}$  is effective radius or the half-light radius. In other words, roughly speaking, the uncertainty in each of the centroid components for a galaxy measured at  $\nu = 10$  is roughly one third of the half-light radius. A more accurate estimate would also consider only the innermost resolved region of galaxies, but given the rough nature of our forecasts we have not considered this here. We have found that the scatter in second moments of galaxy images obeys a similar rough scaling with  $\nu^{-1}$ .

## REFERENCES

- R. E. White, III, W. C. Keel, and C. J. Conselice, *ApJ* **542**, 761 (2000).
- B. W. Holwerda, R. J. Allen, W. J. G. de Blok, A. Bouchard, R. A. González-Lópezlira, P. C. van der Kruit, and A. Leroy, *Astronomische Nachrichten* **334**, 268 (2013), 1209.0306.
- B. T. Draine, D. A. Dale, G. Bendo, K. D. Gordon, J. D. T. Smith, L. Armus, C. W. Engelbracht, G. Helou, R. C. Kennicutt, Jr., A. Li, et al., *ApJ* **663**, 866 (2007), astro-ph/0703213.
- D. Calzetti, *PASP* **113**, 1449 (2001), arXiv:astro-ph/0109035.
- G. Kauffmann, T. M. Heckman, S. D. M. White, S. Charlot, C. Tremonti, J. Brinchmann, G. Bruzual, E. W. Peng, M. Seibert, M. Bernardi, et al., *MNRAS* **341**, 33 (2003), astro-ph/0204055.
- Z. Shao, Q. Xiao, S. Shen, H. J. Mo, X. Xia, and Z. Deng, *ApJ* **659**, 1159 (2007), astro-ph/0611714.
- J. Chevallard, S. Charlot, B. Wandelt, and V. Wild, *MNRAS* **432**, 2061 (2013), 1303.6631.
- C.-W. Yip, A. S. Szalay, S. Carliles, and T. Budavári, *ApJ* **730**, 54 (2011), 1101.5651.
- E. M. Huff, E. Krause, T. Eifler, M. R. George, and D. Schlegel, *ArXiv e-prints* (2013), 1311.1489.
- S. P. Driver, C. C. Popescu, R. J. Tuffs, J. Liske, A. W. Graham, P. D. Allen, and R. de Propris, *MNRAS* **379**, 1022 (2007), 0704.2140.
- M. W. Grootes, R. J. Tuffs, C. C. Popescu, B. Pastrav, E. Andrae, M. Gunawardhana, L. S. Kelvin, J. Liske, M. Seibert, E. N. Taylor, et al., *ApJ* **766**, 59 (2013), 1302.1379.
- M. Boquien, A. Boselli, V. Buat, M. Baes, G. Bendo, S. Boissier, L. Ciesla, A. Cooray, L. Cortese, S. Eales, et al., *A&A* **554**, A14 (2013), 1303.1178.
- M. T. Sargent, C. M. Carollo, P. Kampczyk, S. J. Lilly, C. Scarlata, P. Capak, O. Ilbert, A. M. Koekemoer, J.-P. Kneib, A. Leauthaud, et al., *ApJ* **714**, L113 (2010), 1003.3458.
- Y. I. Byun, K. C. Freeman, and N. D. Kylafis, *ApJ* **432**, 114 (1994).
- E. M. Xilouris, Y. I. Byun, N. D. Kylafis, E. V. Paleologou, and J. Papamastorakis, *A&A* **344**, 868 (1999), astro-ph/9901158.
- S. Bianchi, *A&A* **471**, 765 (2007), 0705.1471.
- D. A. Gadotti, M. Baes, and S. Falony, *MNRAS* **403**, 2053 (2010), 1001.2303.
- R. Massey, C. Heymans, J. Bergé, G. Bernstein, S. Bridle, D. Clowe, H. Dahle, R. Ellis, T. Erben, M. Hettterscheidt, et al., *MNRAS* **376**, 13 (2007), astro-ph/0608643.

- G. M. Bernstein and M. Jarvis, AJ **123**, 583 (2002), arXiv:astro-ph/0107431.
- B. S. Ryden, ApJ **601**, 214 (2004), astro-ph/0310097.
- A. Leauthaud, R. Massey, J.-P. Kneib, J. Rhodes, D. E. Johnston, P. Capak, C. Heymans, R. S. Ellis, A. M. Koekemoer, O. Le Fèvre, et al., ApJS **172**, 219 (2007), astro-ph/0702359.
- C. Heymans, L. Van Waerbeke, L. Miller, T. Erben, H. Hildebrandt, H. Hoekstra, T. D. Kitching, Y. Mellier, P. Simon, C. Bonnett, et al., MNRAS **427**, 146 (2012), 1210.0032.
- The Dark Energy Survey Collaboration, ArXiv Astrophysics e-prints (2005), astro-ph/0510346.
- S. Miyazaki, Y. Komiyama, H. Nakaya, Y. Kamata, Y. Doi, T. Hamana, H. Karoji, H. Furusawa, S. Kawanomoto, T. Morokuma, et al., in *Society of Photo-Optical Instrumentation Engineers (SPIE) Conference Series* (2012), vol. 8446 of *Society of Photo-Optical Instrumentation Engineers (SPIE) Conference Series*.
- J. Rhodes, A. Refregier, and E. J. Groth, ApJ **536**, 79 (2000), astro-ph/9905090.